Investigating the morphology, hardness, and porosity of copper filters produced via HydraulicPressing

Hasan Ayub, Lehar Asip Khan, Eanna McCarthy, Inam Ul Ahad, Karsten Fleischer, Dermot Brabazon

*I-Form, Advanced Manufacturing Research Centre, **&** Advanced Processing Technology Research Centre, School ofMechanical and Manufacturing Engineering, Dublin City University, Glasnevin, Dublin 9, Ireland*

Abstract

This paper presents an examination of the production of copper air filters via the Hydraulic Pressing (HP) method. Processing conditions examined included powder particle type (spherical and dendritic), varying compaction pressures (635, 714, and 793 MPa) anddifferent pore forming (polyvinyl alcohol (PVA)) concentrations (1, 2, and 3 wt.%). Following compaction, the samples were thermally sintered in a two stage sintering regime at 200 °C and 750 °C. The morphology, porosity, and mechanical properties of the sintered samples were characterised. Morphological analysis demonstrated better consolidation and over-lapping of the copper powder particles in samples with a higher weight percentage of thePVA. Highest porosity was achieved in the sample produced using the dendritic copper powder mixed with highest weight percentage of PVA. As the samples were very porous,the hardness of the samples varied greatly. Samples prepared with spherical powders at high pressure demonstrated the highest hardness. The results in this study show that copper filters with 14%e26% porosity can effectively be produced using spherical and dendritic copper powders by controlling the compaction pressure and PVA concentration.

1. Introduction

Minimum scrap losses and near net shaping are benefits of powder compaction which make it a widely utilized sustainable commercial fabrication process. Metal powder processing can be performed by different techniques such as Hydraulic Pressing (HP), spark plasma sintering, and via laser or electron beam-based additive manufacturing. Metal powder processing is utilised in different engineering fields such as in the automotive [1], aerospace [2,3], healthcare [4], tooling [5], and oil and gas [6] industries. Compaction based powder metallurgy is a three step process, including preparation of the powder feedstock, compacting the powder in desired shape, and consolidation via sintering at high temperature [7e13]. Powder metallurgy can be used to fabricate filters with predefined porosities by mixing and processing the metal powder with a porogen. These porogens help the metal powders to move

during consolidation, the metal powder particles to bind and act as temporary space holder. During high temperaturedslu sintering, these porogens are decomposed, thereby creating a porous structure. Polymers such as polyvinyl alcohol (PVA), polymethyl-methacrylate (PMMA), paraformaldehyde (poly-oxymethylene), and inorganic salts, such as sodium chloride (NaCl), magnesium chloride, ammonium bicarbonate, calcium chloride etc. Have been used as binding agents and porogens [14-16]. The selection of porogen is based on meeting of certain criteria, such as decomposition temperature and residual contamination (if any), and shape and size of resulting pores. The presence of voids and high porosity in metals is widely utilized in various industrial applications such as electro-chemical sensors, catalysts, energy storage, and metal filters [17-21]. Porous metals demonstrate durability and high energy absorption characteristics when subject to impact loading. Copper is a good candidate material for structural applications due to its good structural strength and energy absorption capability [5,22,23]. Vincent et al. [24] investigated the effect of porosity on the overall thermal conductivity of copper processed via powder metallurgy. The copper powder was compacted and sintered by hot-pressing at 650 °C. The relationship of pressing time and pressure was studied presenting the volume percentage of porosity. Application of pressure for 20 min lead to approximately 3% porosity. Ros et al. [25] utilized hot isostatic pressing technique and prepared porous copper using NaCl as space holder. NaCl was added up to weight percentage of 40% and decomposed by sintering process. Highest porosity of 27.96% was achieved while thermal conductivity was reduced by 64% comparing to the pure copper. Abu-Qail et al. [26] fabricated copper-tungsten composites using the cold compaction techniques under pressures ranging from 300 to 1200 MPa. Increased density was achieved at higher pressures and copper content. Moreover, improved homogeneity in the structure was observed for longer sintering times up to 2 h. Deepranj et al. [27] performed investigations on the effects of sintering parameters on the hardness of the copper alloy prepared via powder metallurgy. Hydraulic Pressing was used prior to sintering the compacted copper while PVA and water (wetting agent) were used as binders. They concluded that with water as wetting agent a good grain structure was achieved while with PVA higher hardness was observed. Akgul et al. [28] examined porous forms of Cu/Al composites using the powder metallurgy technique of Hydraulic Pressing. They inferred that the compaction pressure did affect the porosity level and that the Cu samples had a lower cooling rate than Al even for the same percentage of porosities. Abhishek and Pushyamitra [29] synthesized copper-titanium porous foams using powder metallurgy for investigating the effects of porosity on mechanical properties. They determined that a higher bending strength of the foams resulted from samples with finer pores.

In this paper, copper air filters were fabricated using Hydraulic Pressing (HP) method and argon furnace sintering. The aim of study was to produce porous copper pallets and perform mechanical and morphological characterization. These porous copper pallets can further be used for air filtration as copper has antibacterial properties. Variations in the level of porogen, compaction pressure, and powder morphology were investigated. The density and integrity of the produced porous copper filters were examined.

2. Materials and methods

In this work, spherical and dendritic type copper powders purchased from Sigma-Aldrich were used to fabricate the filters. The purity of spherical and dendritic Cu powders was 98% and 99.7% respectively and their particle size was ≤45 mm. Further technical and physical properties of both types of copper powders are listed in Table 1. Micrographs of both powders are presented in Fig. 2 (a, b) which were taken using a Zeiss EVO LS-15 SEM. Polyvinyl Alcohol (PVA) powder from Sigma-Aldrich was mixed with the copper powders as a lubricant, binder, and to create defined levels of porosity in the produced filters during the sintering step [30].

To achieve different levels of porosities, PVA was mixed with both types of copper powders at 1, 2, and 3 wt. %. For Cu-PVA samples fabrication, the Hydraulic Pressing (HP) was performed using an Atlas Autotouch 40 Ton Hydraulic Press Fig. 1 (a). A schematic diagram of the press and die are shown in the Fig. 3. PVA mixed copper powders (Cu-PVA) were filled into a 20 mm diameter die, reaching 2 mm thickness in the die. A 0.1 mm gap was kept between die and fitting components for cleaning purposes. An appropriate range of compaction pressures to examine was determined from preliminary trial experiments. The samples were compacted at pressures of 635 MPa, 714 MPa, and 793 MPa. The duration of compaction was 9 min for each sample. The experimental process and sample characterization flow is shown Fig. 1 (c). The full design of experiments is presented in Table 2.

After compaction, the Cu-PVA pallets were sintered using a Lenten Tube Furnace LTF 16 Fig. 1 (b). The samples were sintered in an argon environment to avoid oxidation and contamination. Argon flow rate was kept constant at 1 ml/min from a 1 bar supply pressure during the sintering. The maximum temperature of the furnace was kept at 80% of the melting point of the copper to avoid sample melting. Sintering at such high temperature resulted in evaporation of the PVA from the samples leaving micro porosity in the pallets. The maximum temperature used for sintering was 750°C which was achieved using the sintering profile presented in Fig. 4. The temperature increase and decrease ramp rates used were set at 5°C=min. The samples sintering process was performed in two stages, keeping the sample at 200 °C for 60 min and then at 750 °C for 60 min as shown in Fig. 4.
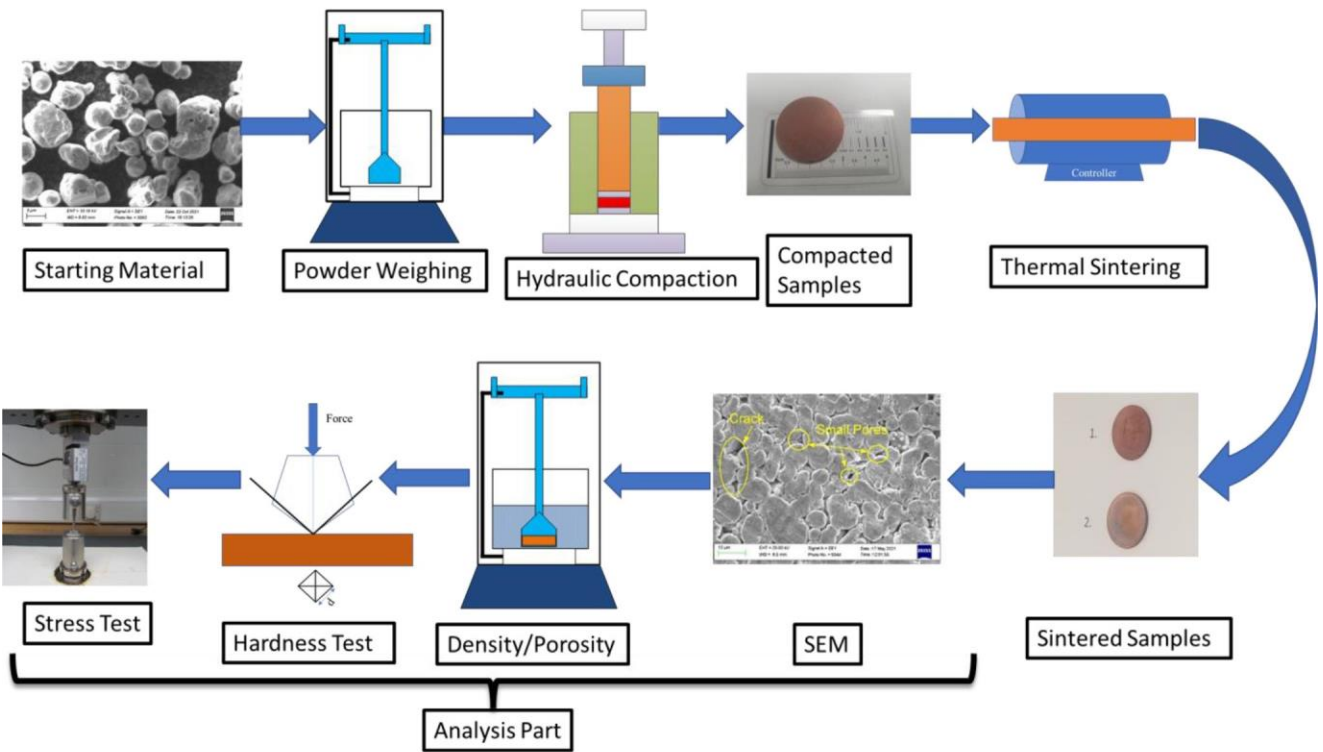
Table 1 e Physical properties of the copper powders employed.				
Product Form	Particle Size (mm)	Purity (%)	Melting/Boiling Point (°C)	Density (Kg/m³)
Powder (Spheroidal)	10e25 mm	98%	1083.4/2567	8960
Powder (Dendritic)	<45 mm	99.7%	1083.4/2567	8960

(a)

(b)

(c)

Fig. 1 - (a) Picture of Atlas Autotouch 40 T Hydraulic Compaction press, (b) picture of Lenton tube heat treatment furnace, and (c) schematic of the experimental sample fabrication procedure and analysis.
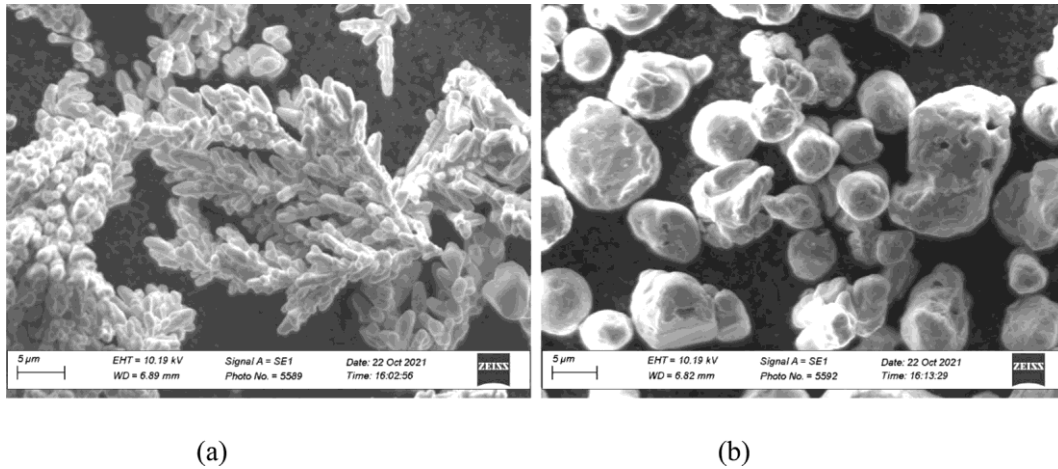
(a)   (b)

Fig. 2 - Microscopic morphology of the (a) dendritic and (b) spheroidal copper powders.

2.1. Morphology analysis

The surface of the samples were imaged at a macroscopic scale with a Leica binocular microscope with a 5 mega pixel digital camera and the micrographs of the compacted and sintered samples were recorded with the Zeiss EVO LS-15 SEM.

2.2. Porosity measurement

Archimedes principle [31], which is widely used method for density measurement, was used to measure the final density of the compacted-sintered Cu-PVA samples. The governing equation for density calculations are presented in the Eq. (1) while Eq. (2) was used to calculate the percentage porosity of the samples.

$$r_s = m_a \frac{r_l}{m_a - m_l} \tag{1}$$

$$4(\%) = \frac{r_s}{r_{Cu}} \times 100 \tag{2}$$

where, r_s and r_{Cu} denote the resulting density of sample and density of pure copper respectively, m_a is the mass of the sample in air, m_l the mass of samples in the liquid, and 4 is the percentage porosity. For each sample three measurements were taken to determine the porosity values.

2.3. Hardness measurement

The resilience of the samples to the mechanical deformation was measured by the Vickers hardness method. A diamond-pyramid-square shaped indenter with an enclosed 136° angle between vertex faces was used. The indentation force of 9.81 N was applied for 20 s on the surface of the samples and the resulting diagonal lengths of the indent were measured. Readings from the diagonal lengths provided the Vickers Pyramid Number (HV) which further lead to the hardness value when used in the Eq. (3).

$$HV = \frac{1.854\,P}{d^2} \tag{3}$$

where, HV is the Vickers Pyramid Number, P is the load measured in Newton, and d denotes the mean diagonal of the indentation.
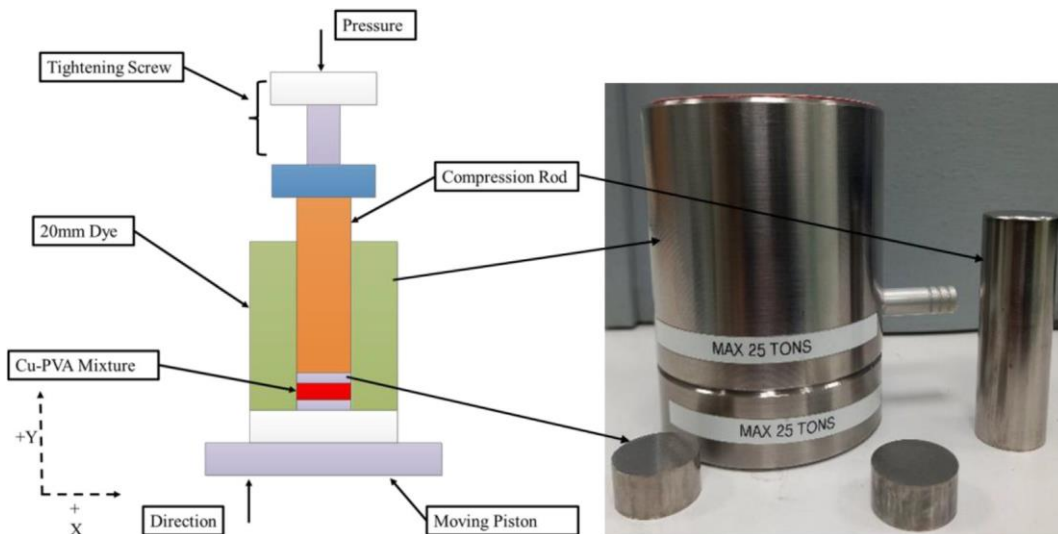

Fig. 3 - Detailed schematic diagram and picture of the hydraulic press.

Table 2 e Powder shape, porogen percentage, and pressure level parameters investigated for powder compaction. All samples were compressed for 9 min and sintered at 200 °C for 60 min and 750 °C for 60 min.			
Sample Number	Powder Shape	PVA (wt. %)	Pressure (MPa)
1	Spherical	1	635
2	Spherical	2	635
3	Spherical	3	635
4	Spherical	1	714
5	Spherical	2	714
6	Spherical	3	714
7	Spherical	1	793
8	Spherical	2	793
9	Spherical	3	793
10	Dendritic	1	635
11	Dendritic	2	635
12	Dendritic	3	635
13	Dendritic	1	714
14	Dendritic	2	714
15	Dendritic	3	714
16	Dendritic	1	793
17	Dendritic	2	793
18	Dendritic	3	793

The hardness values were taken at five different locations on the samples as illustrated in the Fig. 5. For each location on the sample three values of hardness were taken and the result was averaged to reduce the ambiguity.

Further characterization of the samples was performed by indentation testing using 5 mm protrusion indenter on the Zwick Roell, UK universal testing machine (Z005, T1-FR005TN.A50). This test set-up has been previously presented [12,13]. The indentation phenomenon was performed at a loading velocity of 1 mm/min. The radial stress (s_r) and tangential stress (s_t) were calculated via Eqs. (4) and (5) presented using the following equations [32]:

$$s_r = \frac{3F}{2\mathrm{p}t^2}\eth 1 \mathrm{\thorn} n\mathrm{\thorn} log\frac{R}{x} \tag{4}$$

$$s_t = \frac{3F}{2\mathrm{p}t^2}\ \eth 1 \mathrm{\thorn} n\mathrm{\thorn} log\frac{R}{x}\mathrm{\thorn}\eth 1 - n\mathrm{\thorn} \tag{5}$$

where F denotes the vertical load at centre point, x is the indenter diameter, t is the thickness of the sample, n is the Poisson ratio, and R presents the radius of the samples. In current investigations the axial stress is neglected in comparison to the radial and tangential stresses [33].

3. Results and discussion

3.1. Morphological analysis

3.1.1. Spherical powder
The compacted and sintered samples were all robust and stable in structure, see Fig. 6: Sintered samples fabricated from (a) spherical and (b) dendritic copper powder. Fig. 7
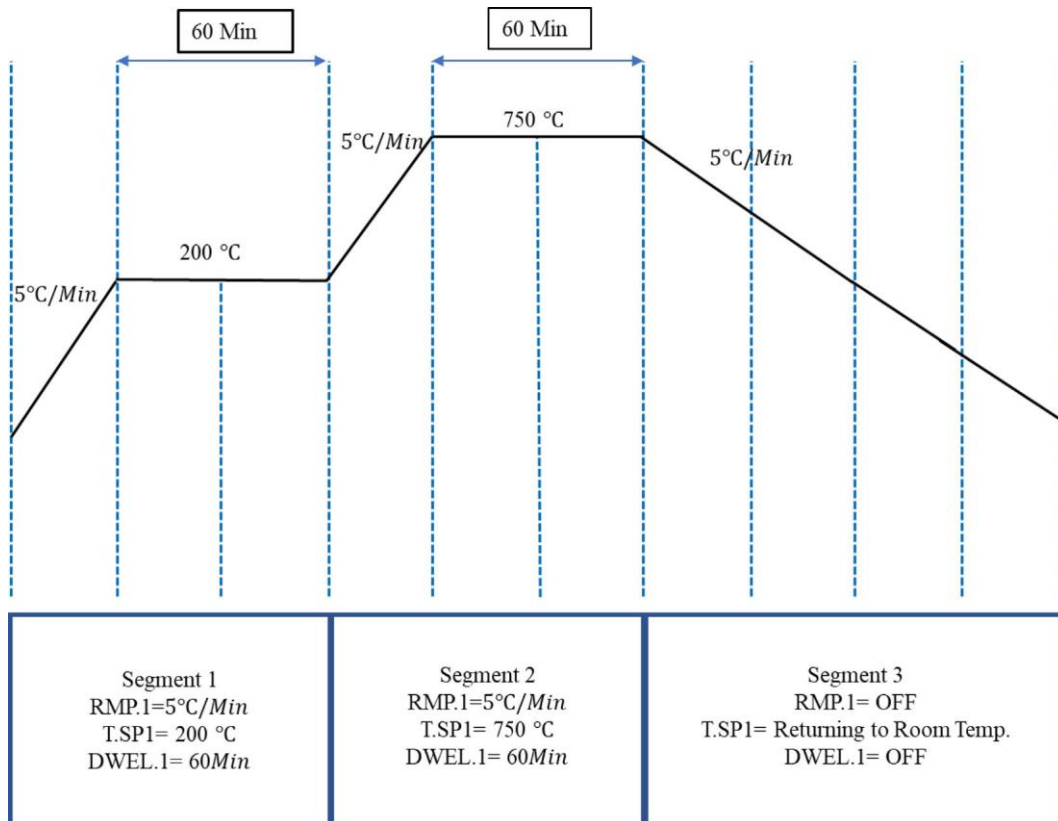

Fig. 4 - Furnace sintering parameters for the compacted copper powders with temperature ramp up, hold, and ramp down timelines shown.
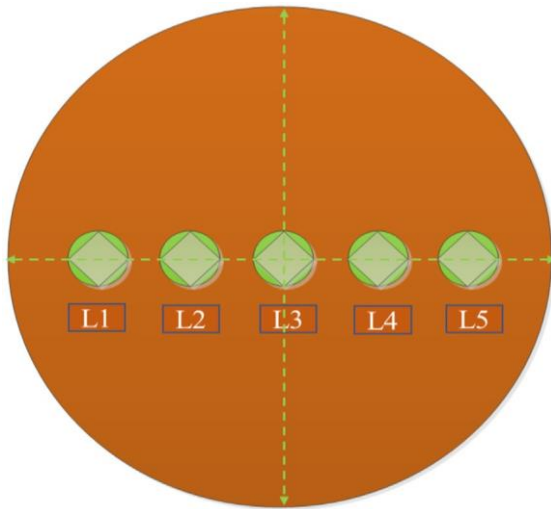
Fig. 5 - Locations on the surface of sample selected for measurement of Vickers hardness.

presents SEM images of the samples produced with the spheroidal copper powder and using three different percentages of the PVA and three compaction pressures. Fig. 7 (a) shows that the lowest percentage of PVA in the copper pellets that was compacted at 635 MPa (i.e., sample 1) resulted in small pores. It was observed that the particles were not fully consolidated into each other and a low level of overlapping of melted particles was achieved. Keeping the compaction and sintering parameters the same and increasing the PVA concentration to 2 wt. % for sample 2 resulted in more consolidation of copper powders and medium sized pores on the surface were observed comparing to the sample 1 (with 1 wt.% PVA). In Fig. 7 (c), with the 3 wt. % PVA, it can be observed that powder particles were fully melted and consolidated into each other. This resulted in overlapping of melted particles and formation of small pores due to removal of PVA during sintering. Fig. 7 (d, e, & f) presents SEM images of 1e3 wt. % PVA mixed with copper

compacted at a pressure of 714 MPa. The SEM image of sample 4 (i.e., 1 wt. % PVA) shows that copper particles were partially melted and consolidated with each other. The overlapping of melted particles was higher comparing to sample 1, and the formation of small pores was observed. Sample 5 (Fig. 7 (e)) shows better consolidation of the copper particles with similar pores as observed in sample 4. Interestingly, in Fig. 7 (f), it was noted that the powder particles consolidated very well with each other. Large and small sized pores were observed. Fig. 7 (g) demonstrates the morphology of the 1% PVA mixed copper compacted disk produced at die holding pressure of 793 MPa. Powder particle overlapping can be seen as well as small pores. Fig. 7 (h) shows uniform pores of equal size with less overlapping, compared to Fig. 7 (g), as a result of increasing PVA concentration to 2 wt. %. A further increase in the PVA wt. % in the copper powder to 3 wt. % resulted in better consolidation of the particles which resulted in very few small pores.

3.1.2. Dendritic powder

The samples compacted and sintered from the dendritic copper powder showed a different pore size and porosity trend comparing to that from the spherical shaped powder. Fig. 8 presents the SEM micrographs for these samples. Fig. 8 (a) presents the micrograph of the powder compacted with 635 MPa and 1 wt.% of PVA. This sample contained a good consolidation of the particles with significant number of pores present. Increasing the PVA to 2 wt.% as shown in Fig. 8 (b) resulted in a very uniform particle consolidation and distributed porosity. The SEM micrographs for samples prepared at 714 MPa pressure for 9 min and sintered at same parameters are presented in Fig. 8 (d), (e), and (f). Fig. 8 (g, h, & i) shows SEM results of the dendritic shape copper sample pressed at a compaction pressure of 793 MPa. Fig. 8 (g) presents 1 wt. % PVA mixed copper pellet compact at the highest die holding pressure used in this study. The increase in pressure resulted in a high density in the pellet. Small sized pores also appeared on the surface of the pellet. The powder particles melted and bonded well with the other particles. In Fig. 8 (b), the PVA concentration was increased to 2 wt. %, which resulted in the
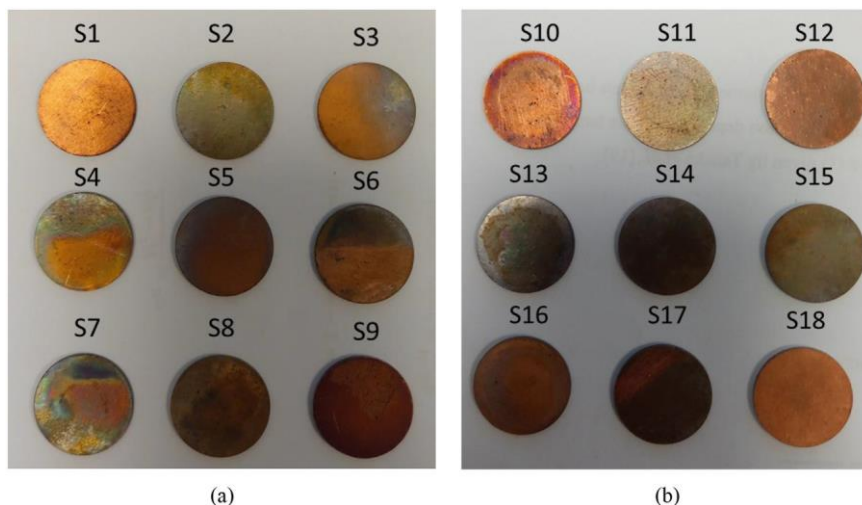

Fig. 6 - Sintered samples fabricated from (a) spherical and (b) dendritic copper powder.
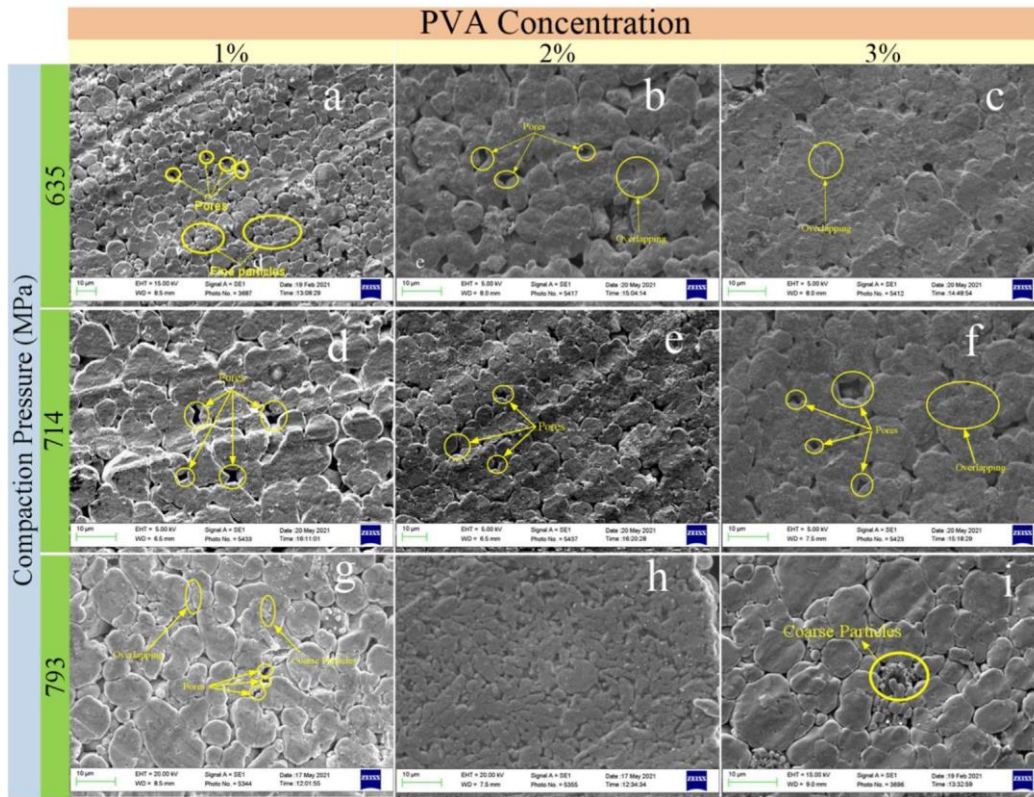
Fig. 7 - Micrographs of the compacted and sintered filters produced using the spheroidal powder.
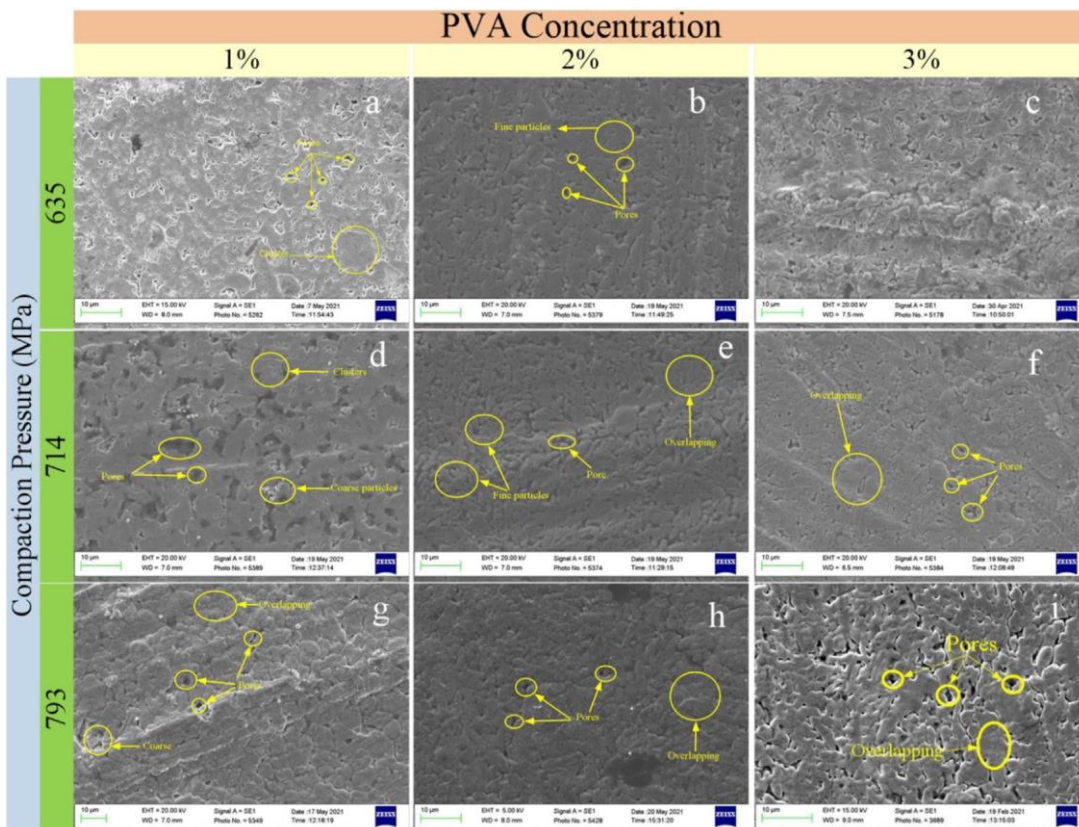

Fig. 8 - Micrographs of compacted and sintered filters produced using the dendritic power.

Measurement Location	S1	S2	S3	S4	S5	S6
	Spherical; Compaction at 635 MPa			Spherical; Compaction at 714 MPa		
L1	75.4	71.9	62	68.8	68.3	48.2
L2	68.3	57.1	89.2	57	52.4	71.3
L3	49.8	55.1	84.3	51.5	98	116
L4	70.2	53.1	67	70.5	96.2	46.7
L5	89.6	67	61	67.3	61.3	49.2
Avg.	70.7	70.6	72.7	63.0	75.2	66.3
	S7	S8	S9	S10	S11	S12
	Spherical; Compaction at 793 MPa			Dendritic; Compaction at 635 MPa		
L1	61.3	95.8	100	68	105	84.3
L2	53.3	74.2	63.6	74	111	90
L3	118	116	114	71.3	55.1	98.5
L4	57.1	105	61.5	68	95.8	90.8
L5	66	101	91.6	67.8	100	83.9
Avg.	71.1	98.4	82.75	69.8	93.4	89.5
	S13	S14	S15	S16	S17	S18
	Dendritic; Compaction at 714 MPa			Dendritic; Compaction at 793 MPa		
L1	95.8	83.9	95.8	48.2	97.6	66
L2	86.9	74.2	100	57.1	95.8	55.1
L3	68.6	71	98	95.8	74.2	80.2
L4	95.3	96.2	102	55.3	87.6	54.2
L5	86.1	98.9	94.9	51.5	88.4	61.3
Avg.	86.5	84.8	98.1	61.6	88.7	63.4

Table 3 - Hardness results measured from the surface of the copper disks produced with the spherical and dendritic copper powders.

formation of some pores on the surface of the pallet. In Fig. 8 (c), with the addition of PVA to copper, there was more porosity as anticipated.

3.2. Porosity measurements

Different percentages of PVA were added in the copper powder to intentionally introduce porosity in the final compacted-sintered copper pellets. The density of the samples measured using Archimedes principle was subsequently used to calculating the percentage of porosity in the samples. The percentage of porosity for the samples produced using the spheroidal powder under the different operating parameters,
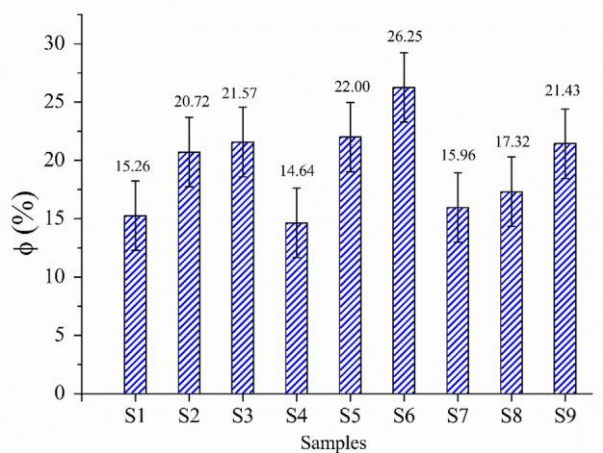
Fig. 9 - Porosity of the Cu-PVA samples produced with spheroidal powder. For samples 1 to 9; n ¼ 3; error bars are 95% CI.

as listed in Table 3, is presented in Fig. 9. An interesting phenomenon observed in Fig. 9 is that the porosity was increasing with the increase in the PVA concentration for each set of samples, which was also previously reported [34]. For first set of the samples (i.e., S1-S3) the percentage porosity achieved was 21.57% with 3% PVA. For samples S4-S6, the porosity increases almost linearly with increasing PVA content. Moreover, for the maximum pressure (i.e., S7-S9), the porosity increased from 15.96% to 21.43%. Similarly, Fig. 10 presents the porosity results for dendritic type Cu-PVA samples prepared and sintered using the same compaction and sintering operating parameters as for the spheroidal samples. In the dendritic type samples, the percentage of porosity followed the same trend as in the spheroidal samples in terms of

Fig. 10 - Porosity of the Cu-PVA samples produced with dendritic powder. For samples 10 to 18; n ¼ 3; error bars 95% CI.
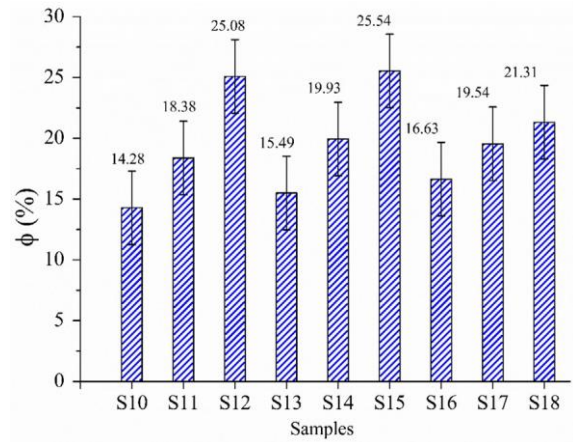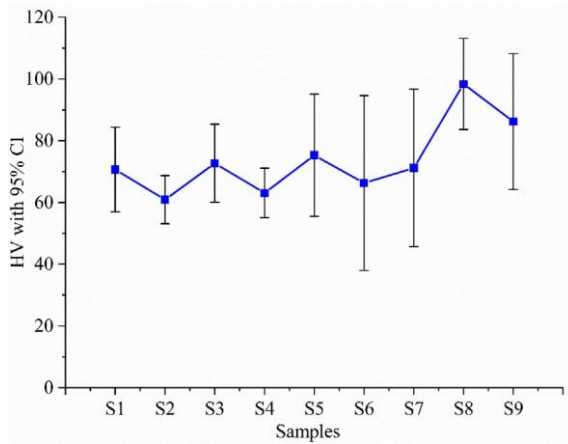
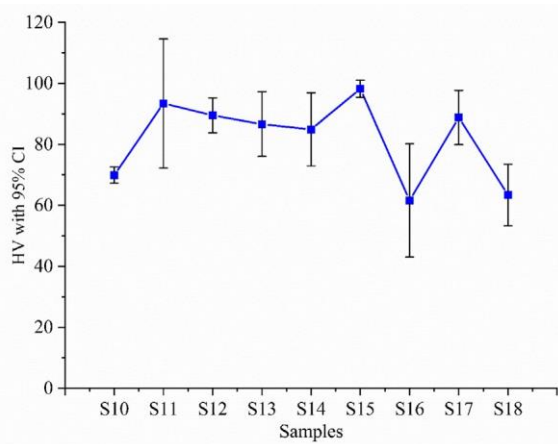Fig. 11 - Average hardness values with error bars at 95% confidence intervals shown for S1-S9, n ¼ 5.

Fig. 12 - Average hardness values with error bars at 95% confidence intervals shown for S10eS18, n ¼ 5.

its increase with increasing PVA concentration. It is interesting to observe that for the compaction pressures of 20.5 T and 22.5 T (i.e., S10-S12 & S13-S15) the increase in the porosity follows an almost linear trend. Within this study, the maximum average porosity of 26.25% was found in the spheroidal sample S6 which was produced at the highest PVA content and intermediate pressure level.

3.3. Hardness results

Mechanical integrity is an important aspect to measure when designing porous material which can be measured by mechanical testing methods such as Vickers hardness test. In the present study, the Vickers hardness was used to measure the hardness of the Cu-PVA sintered samples. The hardness values were taken at five different locations on each sample as illustrated in the Fig. 5 and the results are summarised in Table 3. Among the five locations on the sample surface, the hardness values change abruptly which suggests that local porosity had a significant effect on this macroscopic hardness measurement. The SEM images confirmed also that porosity was well distributed with in the samples. For example, in sample S1 (spheroidal powder sample), the hardness values ranged from 49.8 HV in the middle to 89 HV toward the sample edge. However, for S5, the middle locations had highest hardness (98 HV) for the sample compared to a much lower hardness at the edge (61 HV). Similar observations were also made by Cherry et al. [35] where more porous samples showed lower hardness. Varied hardness values across the sample are also noted and reported in Table 3 for the samples produced from the dendritic copper powder. Considering the compaction force, the samples produced with the spherical powder demonstrated comparatively higher hardness at 793 MPa compaction pressure whereas in dendritic powder samples, the highest average hardness was measured from the samples compacted at the intermediary compaction pressure of 714 MPa. The lowest and highest hardness values measured were 48 HV and 118 HV (i.e., S12 and S13 respectively). Overall,
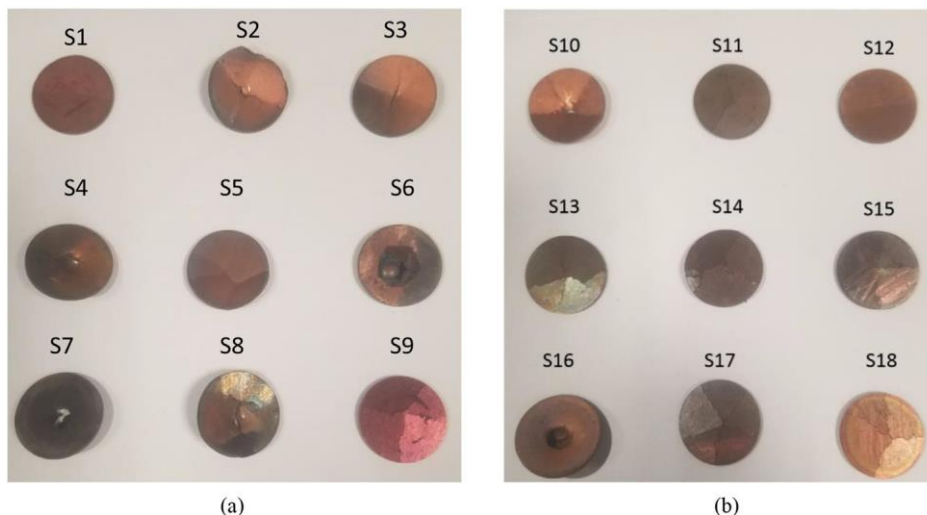

Fig. 13 - Samples after indentation testing produced from (a) spheroidal powder samples (S1-S9) and (b) dendritic powder samples (S10-S18).
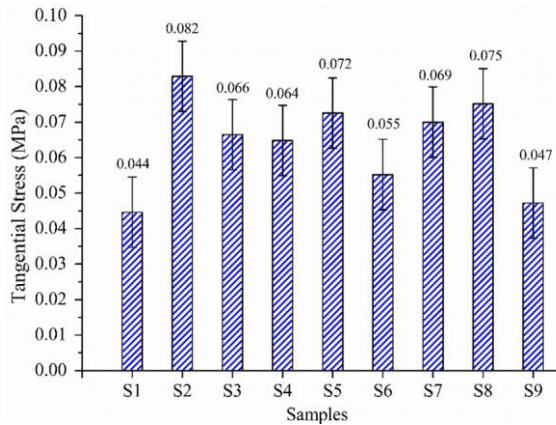
Fig. 14 - Experimental results for indentation testing of spheroidal samples (S1-S9) for tangential stress with error bars at 95% confidence interval.
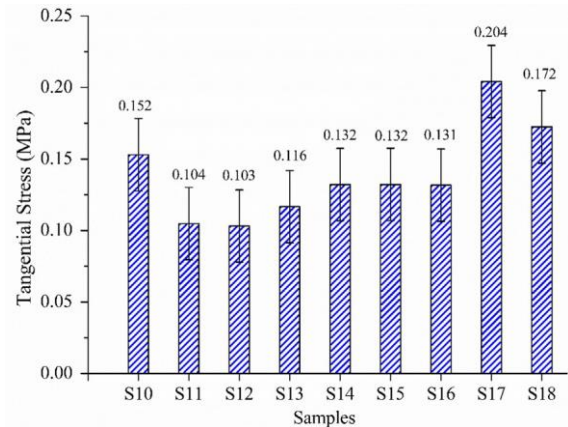

Fig. 16 - Experimental results for indentation testing of dendritic samples (S10-S18) for tangential stress with error bars 95% confidence interval.

considering the 14%-25% porosity in the produced samples, they showed good hardness results comparing to annealed copper samples which are reported as having 57 HV [36,37]. Moreover, the Fig. 11 and Fig. 12 present the 95% confidence interval around the average HV value for each sample (i.e., S1-S18).

3.4. Results from indentation testing of samples

Fig. 14-17 present the corresponding radial and tangential stresses for all samples. Tested samples after indentation tests are presented in Fig. 13. Fig. 14 presents the indentation test results for Spheroidal type samples (i.e., S1-S9) for the peak tangential stress induced on the samples. Observing the results, a random peak stress was seen by the samples ranging from maximum of 0.082 MPa and minimum peak stress of 0.044 MPa. Highest tangential peak stress was observed S2 while minimum peak stress was seen in S1. Further, the radial stresses were also calculated for samples S1-S9 presented in the Fig. 15. The peak radial stresses were significantly lower than the tangential stresses. The minimum peak radial stress
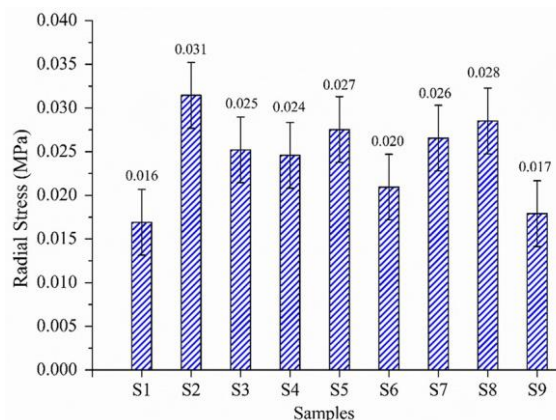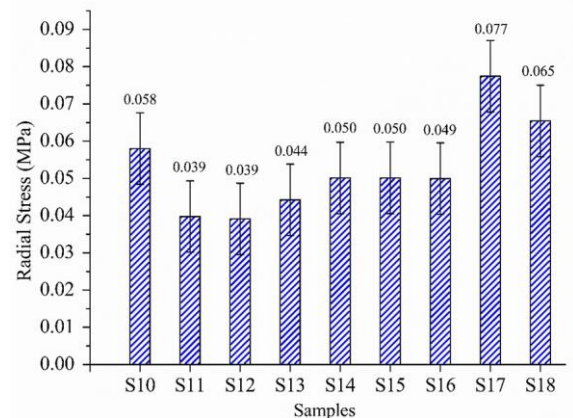

Fig. 17 - Experimental results for indentation testing of dendritic type samples (S10-S18) for radial stress with error bars at 95% confidence interval.

was 0.044 MPa while maximum achieved was 0.082 MPa for same samples (S2 and S1). Peak tangential and radial stresses observed in the dendritic type samples (i.e., S10-S18) are graphed in Fig. 16, Fig. 17). The dendritic type showed significantly high peak tangential stress comparing to the spheroidal type samples. Similar to the samples S1-S9 a random pattern of peak stresses was seen for tangential and radial stresses. A peak tangential stress of 0.204 MPa was absorbed by samples S17. The peak tangential stresses for dendritic type samples were 59.8% higher than observed in the spheroidal samples. Furthermore, the radial peak stresses in S10-S18 also showed similar random pattern with the highest peak 0.077 MPa.

Fig. 15 - Experimental results for indentation testing of spheroidal samples (S1-S9) for radial stress with error bars at 95% confidence interval.

4. Conclusions

The copper filters were produced with spherical and dendritic copper powders using the HP and thermal sintering. Both types of powders demonstrated similar results in morphology,

porosity, and hardness profile. However, the change in weight percentage of the porogen PVA and use of different compaction pressures resulted in formation of filters with different morphological characteristics and levels of porosity. PVA acted as binding agent for the HP produced copper green compact and as an agent which was demonstrated to be useful for achieving a definable level of porosity within the produced disk filters. Due to this dual role, interesting results were observed by changing the PVA weight percentage from 1% to 3%. With increasing concentration of PVA, the powders were better consolidated and more overlapping of the copper particles was observed in the filter surface micrographs. The samples prepared with 2 wt. % PVA demonstrated more fine pores as compared to larger pores observed in the samples prepared with 1 wt. % PVA. Copper filters produced with 3 wt. % PVA demonstrated good overlapping and well distributed pores across the samples. Interestingly, the compaction pressure had no or very minor influence on the porosity of the samples. However, with increasing PVA concentration, higher porosity levels were achieved. The highest porosity was achieved in the samples compressed at the intermediary pressure of 714 MPa and with the highest level of PVA. With the processing conditions used in this study, air flow filters can be produced using copper powders with porosities between 14% and 25%. Lastly, the indentation testing was performed in the samples which revealed the level of peak stresses absorbed by the samples. Peak tangential and radial stress absorbed by the dendritic type samples was 60% higher on average compared to the spheroidal samples. This result is considered to be due to the increased interlocking of the dendrite arms and resulting better bonding during sintering. Further work to improve the strength and perhaps the anti-bacterial or anti-viral nature of this filter production method could investigate the use graphene or carbon nanotube reinforced copper matrix composites [38].

Declaration of Competing Interest

The authors declare the following financial interests/personal relationships which may be considered as potential competing interests: Hasan Ayub reports financial support was provided by Science Foundation Ireland.

Acknowledgments

R E F E R E N C E S

[1] Kianian B. Comparing acquisition and operation life cycle costs of powder metallurgy and conventional wrought steel gear manufacturing techniques. Procedia CIRP 2019;81:1101-6. https://doi.org/10.1016/j.procir.2019.03.260.

[2] qiang Tan Z, Zhang Q, yi Guo X, jiang Zhao W, shang Zhou C, Liu Y. Recent developments in powder metallurgy based aluminium alloy composite for aerospace applications. J Cent South Univ 2020;27(6):1611-23. https://doi.org/10.1007/s11771-020-4394-y.

[3] Vasanthakumar P, Sekar K, Venkatesh K. Recent developments in powder metallurgy based aluminium alloy composite for aerospace applications. Mater Today Proc 2019;18:5400-9. https://doi.org/10.1016/j.matpr.2019.07.568.

[4] Nazari KA, Nouri A, Hilditch T. Mechanical properties and microstructure of powder metallurgy Ti-xNb-yMo alloys for implant materials. Mater Des 2015;88:1164-74. https://doi.org/10.1016/j.matdes.2015.09.106.

[5] Ja-ye S, Do-sik S. Compressive behavior of porous materials fabricated by laser melting deposition using AlSi12 powder and foaming agent. Mater Res Express 2019;6(1). https://doi.org/10.1088/2053-1591/aafc5a. 0-31.

[6] Bjurström M, Powdermet S, Sandvik CH, Ab P. PVP2009-77787 PVP2009-77787 FINAL producing HP pump barrels utilizing powder metallurgy and hot isostatic. 2009. p. 1-7.

[7] Liu B, Liu Y, He XY, Tang HP, Chen LF, Huang BY. Preparation and mechanical properties of particulate-reinforced powder metallurgy titanium matrix composites. Metall. Mater. Trans. A Phys. Metall. Mater. Sci. 2007;38(11):2825e31. https://doi.org/10.1007/s11661-007-9329-9.

[8] Čapek J, Vojtěch D. Properties of porous magnesium prepared by powder metallurgy. Mater Sci Eng C 2013;33(1):564-9. https://doi.org/10.1016/j.msec.2012.10.002.

[9] Zhang ZW, Liu ZY, Xiao BL, Ni DR, Ma ZY. High efficiency dispersal and strengthening of graphene reinforced aluminum alloy composites fabricated by powder metallurgy combined with friction stir processing. Carbon N. Y. 2018;135:215e23. https://doi.org/10.1016/j.carbon.2018.04.029.

[10] Bolzoni L, Ruiz-Navas EM, Gordo E. Quantifying the properties of low-cost powder metallurgy titanium alloys. Mater Sci Eng, A 2017;687:47-53. https://doi.org/10.1016/j.msea.2017.01.049. 2016.

[11] Fang ZZ, Paramore JD, Sun P, Chandran KSR, Zhang Y, Xia Y, et al. Powder metallurgy of titanium-past, present, and future. Int Mater Rev 2018;63(7):407-59. https://doi.org/10.1080/09506608.2017.1366003.

[12] Liu J, Silveira J, Groarke R, Parab S, Singh H, McCarthy E, et al. Effect of powder metallurgy synthesis parameters for pure aluminium on resultant mechanical properties. Int J Material Form 2019;12(1):79-87. https://doi.org/10.1007/s12289-018-1408-5.

[13] Liu J, Khan U, Coleman J, Fernandez B, Rodriguez P, Naher S, et al. Graphene oxide and graphene nanosheet reinforced aluminium matrix composites: powder synthesis and prepared composite characteristics. Mater Des 2016;94:87-94. https://doi.org/10.1016/j.matdes.2016.01.031.

[14] Hangai Y, Zushida K, Fujii H, Ueji R, Kuwazuru O, Yoshikawa N. Friction powder compaction process for fabricating open-celled Cu foam by sintering-dissolution process route using NaCl space holder. Mater Sci Eng, A 2013;585:468e74. https://doi.org/10.1016/j.msea.2013.08.004.

[15] Rodriguez-Contreras A, Punset M, Calero JA, Gil FJ, Ruperez E, Manero JM. Powder metallurgy with space holder for porous titanium implants: a review. J Mater Sci Technol 2021;76:129e49. https://doi.org/10.1016/j.jmst.2020.11.005.

[16] Jia J, Jing Y, Liu D, Ju J, Wang X, Ji G. Compressive properties of porous Cu reinforced by inserting copper pillars or tubes. J Porous Mater 2021;28(3):963-72. https://doi.org/10.1007/s10934-021-01049-5.

[17] Wang H, Hu X, Ke Z, Du CZ, Zheng L, Wang C, et al. Review: porous metal filters and membranes for oil-water

separation. Nanoscale Res Lett 2018;13. https://doi.org/10.1186/s11671-018-2693-0.

[18] Tuchinskiy L. Novel manufacturing process for metal and ceramic microhoneycombs. Adv Eng Mater 2008;10(3):219-22. https://doi.org/10.1002/adem.200700268.

[19] Zhang J, Li CM. Nanoporous metals: fabrication strategies and advanced electrochemical applications in catalysis, sensing and energy systems. Chem Soc Rev 2012;41(21):7016-31. https://doi.org/10.1039/c2cs35210a.

[20] Li WQ, Guo SJ, Tan L, Liu LL, Ao W. Heat transfer enhancement of nano-encapsulated phase change material (NEPCM) using metal foam for thermal energy storage. Int J Heat Mass Tran 2021;166. https://doi.org/10.1016/j.ijheatmasstransfer.2020.120737.

[21] Khan LA, Khan MM, Ahmed HF, Irfan M, Brabazon D, Ahad IU. Dominant roles of eccentricity, fin design, and nanoparticles in performance enhancement of latent thermal energy storage unit. J Energy Storage 2021;43:103181. https://doi.org/10.1016/j.est.2021.103181. February.

[22] Wang B, Zhang E. On the compressive behavior of sintered porous coppers with low-to-medium porosities-Part II: preparation and microstructure. Int J Mech Sci 2008;50(3):550e8. https://doi.org/10.1016/j.ijmecsci.2007.08.003.

[23] Sabzevari M, Sajjadi SA, Moloodi A. Physical and mechanical properties of porous copper nanocomposite produced by powder metallurgy. Adv Powder Technol 2016;27(1):105e11. https://doi.org/10.1016/j.apt.2015.11.005.

[24] Vincent C, Silvain JF, Heintz JM, Chandra N. Effect of porosity on the thermal conductivity of copper processed by powder metallurgy. J Phys Chem Solid 2012;73(3):499e504. https://doi.org/10.1016/j.jpcs.2011.11.033.

[25] Kadir RAA, Shaari NS, Kamardin K, Bin Khalid MFS, Ismail MH. Thermal properties of porous copper using NaCl as a space holder, vol. 46. Springer Singapore; 2021.

[26] Abu-Oqail A, Ghanim M, El-Sheikh M, El-Nikhaily A. Effects of processing parameters of tungsten-copper composites. Int J Refract Metal Hard Mater 2012;35:207-12. https://doi.org/10.1016/j.ijrmhm.2012.02.015.

[27] Deepanraj B, Senthilkumar N, Tamizharasan T. Sintering parameters consequence on microstructure and hardness of copper alloy prepared by powder metallurgy. Mater Today Proc 2021;xxxx. https://doi.org/10.1016/j.matpr.2021.06.389.

[28] Akgul B, Erden F, Ozbay S. Porous Cu/Al composites for cost-effective thermal management. Powder Technol 2021;391:11e9. https://doi.org/10.1016/j.powtec.2021.06.007.

[29] Sharma A, Mishra P. Microstructure and mechanical behaviour of Ti-Cu foams synthesized via powder metallurgy technique. Mater Res Express 2021;8(3). https://doi.org/10.1088/2053-1591/abed69.

[30] Zairani NAS, Jaafar M, Ahmad N, Abdul Razak K. Fabrication and characterization of porous b-tricalcium phosphate scaffolds coated with alginate. Ceram Int 2016;42(4):5141-7. https://doi.org/10.1016/j.ceramint.2015.12.034.

[31] Lee JC, Ahn SH. Bulk density measurement of porous functionally graded materials. Int J Precis Eng Manuf 2018;19(1):31e7. https://doi.org/10.1007/s12541-018-0004-4.

[32] Hearn EJ. Mechanics of materials. Mech Mater 1993;16(1-2). https://doi.org/10.1007/978-1-4757-1223-0_16.

[33] Timoshenko SP. Theory of plates and shells, vol. 568. McGraw-Hill Classic Textbook Reissue Series); 1964.

[34] Devavarapu S, Chaudhuri P, Shrivastava A, Bhattacharyya S. Processing of porous alumina by foaming method-effect of foaming agent, solid loading and binder. Ceram Int 2019;45(9):12264-73. https://doi.org/10.1016/j.ceramint.2019.03.139.

[35] Cherry JA, Davies HM, Mehmood S, Lavery NP, Brown SGR, Sienz J. Investigation into the effect of process parameters on microstructural and physical properties of 316L stainless steel parts by selective laser melting. Int J Adv Manuf Technol 2015;76(5-8):869-79. https://doi.org/10.1007/s00170-014-6297-2.

[36] Baskoro AS, Supriadi S, Dharmanto. Review on plasma atomizer technology for metal powder. MATEC Web Conf 2019;269:5004. https://doi.org/10.1051/matecconf/201926905004.

[37] Alawadhi MY, Sabbaghianrad S, Huang Y, Langdon TG. Direct influence of recovery behaviour on mechanical properties in oxygen-free copper processed using different SPD techniques: HPT and ECAP. J Mater Res Technol Oct. 2017;6(4):369-77. https://doi.org/10.1016/J.JMRT.2017.05.005.

[38] Dasari BL, Morshed M, Nouri JM, Brabazon D, Naher S. Mechanical properties of graphene oxide reinforced aluminium matrix composites. Compos B Eng 2018;145:136e44. https://doi.org/10.1016/j.compositesb.2018.03.022. October 2017.